ACS EARTH AND SPACE CHEMISTRY

http://pubs.acs.org/journal/aesccq

Article

Temperature-Dependent Phase Transitions of Aqueous Aerosol Droplet Systems in Microfluidic Traps

Priyatanu Roy, Liora E. Mael, Iaroslav Makhnenko, Robert Martz, Vicki H. Grassian, and Cari S. Dutcher*

Cite This: *ACS Earth Space Chem.* 2020, 4, 1527−1539

Read Online

ACCESS | Metrics & More | Article Recommendations | Supporting Information

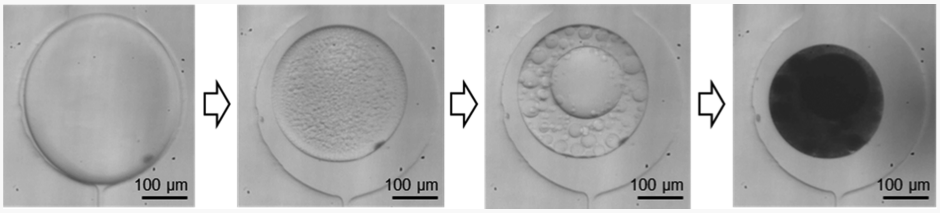

ABSTRACT: Well-mixed atmospheric aqueous aerosol droplets containing multiple chemical species can undergo processes such as liquid−liquid phase separation (LLPS) and crystallization depending on the ambient temperature and relative humidity (RH). So far, only a handful of single droplet studies have examined the effect of temperature in conjunction with the organic to inorganic ratio (OIR) on the separation RH for LLPS. In this work, we present a temperature-controlled microfluidic static trap approach to study the LLPS and efflorescence phenomenon in multiple ternary systems in a quasi-equilibrium manner. Ammonium sulfate or sodium chloride is used as the inorganic phase and 3-methylglutaric acid (3-MGA), poly(ethylene glycol), poly(propylene glycol), or poly(ethylene glycol) diacrylate is used as the organic phase. Results show a clear trend in droplets containing 3-MGA with either salt of the initial LLPS and efflorescence events occurring at higher RH at lower temperatures, while this trend is less obvious for the other organics. The organic to inorganic ratio (OIR) of the system also affected the type of first phase transition, which can be either LLPS or efflorescence. Finally, the rate of RH change also had an impact on the temperature dependence of the formation of either anhydrous or dihydrous crystals of sodium chloride upon efflorescence. These results help inform the effects of temperature, OIR, and rate of RH change on the phase state of aqueous aerosol droplets containing multiple species.

KEYWORDS: *model aerosols, organic to inorganic ratio, liquid−liquid phase separation, microfluidics, temperature-dependent, dehydration rate, separation relative humidity*

INTRODUCTION

Atmospheric aerosols are complex chemical systems subject to a varied range of ambient conditions.[1−3] These particles play a key role in the earth's climate directly by controlling the absorption and scattering properties of the atmosphere[4] or indirectly through forming clouds by acting as cloud condensation nuclei (CCN).[5,6] Unfortunately, aerosols are also the largest source of uncertainty in predictive models for climate change.[7] A single aerosol particle can contain a multitude of chemically distinct components depending on its origin, including inorganic salts; volcanic ash or dust; combustion products; organic acids, bases, or even microorganisms; and biological byproducts.[3,8−15]

In addition to chemical complexity, aerosol particles in the atmosphere can exist in multiple overall phase states classified according to their viscosity as liquid, semisolid, and solid[1,16] or according to their internal phase morphology as mixed, liquid−liquid phase separated (LLPS), and partially or fully effloresced.[16−18] LLPS occurs according to the equilibrium conditions among the separated or mixed phases in an aerosol. Particles can transition among these states depending on their chemical composition along with ambient conditions, such as temperature and relative humidity (RH). LLPS and efflorescence/deliquescence of particles play a crucial role in aerosol properties, such as their optical properties,[19,20] hygroscopicity,[16,21] and heterogeneous chemistry including atmospheric aging or uptake of gas-phase molecules like N_2O_5.[22,23] Additionally, the phase state of a particle can also influence its surface properties and hence its ability to activate into a CCN[24] or ice nucleating capabilities.[25−27]

Methods to quantitatively measure the phase state of aerosol particles include bulk measurements in cases where the separation relative humidity (SRH) of the particle is higher

Received: May 4, 2020
Revised: July 29, 2020
Accepted: August 20, 2020
Published: August 20, 2020

https://dx.doi.org/10.1021/acsearthspacechem.0c00114
ACS Earth Space Chem. 2020, 4, 1527−1539

than the deliquescence relative humidity (DRH). However, this is a rare occurrence, and supersaturation is needed to study LLPS in most relevant aerosol systems. Supersaturation can be achieved in single-particle phase state measurements at the supermicron scale using optical microscopy on droplets on a substrate,[28] electrodynamic balancing,[29] or optical traps.[30] Submicron-scale single-particle phase can be studied using scanning electron microscopy with energy-dispersive X-ray analysis,[31] transmission electron microscopy,[32] and scanning transmission X-ray microscopy/near-edge X-ray absorption fine structure methods.[33] Phases of larger populations of particles can be measured directly using particle water uptake and growth in hygroscopicity tandem differential mobility analyzers,[34−36] microresonators,[37] interdigitated electrodes,[38] and quartz crystal microbalances[39] or indirectly by measuring particle bounce using impactors.[40−43] A comprehensive review by McMurry et al.[44] lists most physical and chemical characterization techniques used for submicron aerosols. The substrate used in contact-based methods can influence the particle morphology during the initial impaction as well as phase transitions. Hydrophobic surfaces are commonly used to minimize this effect. Single-particle trap-based methods often require highly complex instrumentation to obtain measurements and can become cost-prohibitive and time-consuming.

Recently, microfluidic measurements have been used to look at statically trapped single-particle phase transitions[45−47] and ice nucleation.[48] Aerosol droplets are trapped in microfluidic wells that are surrounded by a thin layer of carrier fluid and sandwiched between highly permeable poly(dimethylsiloxane) (PDMS) and nonpermeable glass layers. Morphological changes including LLPS and efflorescence can be observed as droplets evaporate slowly over time in a quasi-equilibrium manner and the changes are recorded in a time-lapse video. Microfluidics offers an advantage over the substrate-based methods since the droplets are encased in a layer of liquid and hence reduce the probability of heterogeneous nucleation from a solid substrate. It also provides a two-dimensional (2D) Hele-Shaw-type geometry, which makes it easier to determine LLPS and the resultant morphology using optical microscopy. In addition, there is usually no need for external relative humidity control during an experiment as the drying process occurs slowly until the droplet RH equilibrates with the surrounding RH. By careful design of flow channels and wells, it is even possible to rehydrate droplets or control the dehydration and rehydration rate by flowing water through channels adjacent to the trapped droplets.[45,49] The disadvantages of this method are that droplet dehydration usually takes a long time, on the order of days. So, the collection of a large number of data points can be challenging. Also, the droplet RH needs to be calculated based on droplet concentration using equilibrium thermodynamic models as direct measurement of water activity or RH in a microfluidic well is not readily feasible.

Factors including temperature as well as the initial composition of a mixed organic−inorganic liquid droplet itself can decide whether an aerosol droplet undergoes LLPS and at what SRH. Among the chemical composition aspects, a universally acknowledged key factor is the oxygen to carbon ratio (O/C) of the organic component.[50−52] Other factors that have been studied are sulfate ratios, molecular weight of the organic,[53] multiple organics,[54] and secondary organic aerosols created from atmospheric aging[55] of the primary aerosols. Certainly, not all systems undergo LLPS before efflorescence. You et al.[53] showed that particles with O/C below 0.57 readily undergo LLPS, whereas particles with O/C between 0.83 and 0.57 undergo LLPS only for certain organics, and particles with O/C above 0.83 do not undergo LLPS. A recent study by Ott et al.[56] on ternary aerosols with added sucrose has expanded the upper limit of the O/C ratio for LLPS to 0.92. Results from more complex systems with more than three components and field samples also agree with this narrow range of O/C necessary for LLPS.[50,54,55]

However, while the effect of chemical composition on LLPS is becoming more extensively understood, the effect of temperature on LLPS is less well-characterized. It was theorized that droplet viscosities at lower temperatures in the troposphere (<298 K) would increase and lead to inhibition of phase separation.[57] In contrast, a recent study on the effect of low temperatures down to 244 K showed that for most of the systems that do undergo LLPS at room temperature, inhibition of LLPS was not noticeable, i.e., SRH was not dependent on the droplet temperature. Furthermore, in some cases, the SRH even increased with a reduction in temperature.[53] Organic to inorganic mass ratio (OIR) of the aerosol also plays a part in the morphology of these phase transitions and generally varies between 0.2 and 3.5 in atmospheric particles.[58−60]

In addition to LLPS, the crystal structure and subsequently the morphology of the aqueous droplet upon efflorescence have also been known to depend upon temperature and drying conditions, specifically, the dehydration rate. Sodium chloride forms two possible crystal structures upon efflorescence, namely, anhydrate ($NaCl_{(s)}$) and dihydrate ($NaCl{\cdot}2H_2O_{(s)}$). The equilibrium phase diagram shows that at temperatures above 0 °C, the $NaCl_{(s)}$ form and below 0 °C, the $NaCl{\cdot}2H_2O_{(s)}$ form are thermodynamically favorable.[18] However, in experiments on droplets on a substrate, it was shown that only $NaCl_{(s)}$ is formed at temperatures as low as −20 °C.[61] In another study,[25] the range of temperatures where the transition from $NaCl_{(s)}$ to $NaCl{\cdot}2H_2O_{(s)}$ occurs was found to be between about −20 °C, where 0% of the particles were in the dihydrate form, and −32 °C, where 100% of the particles observed were the dihydrate. Another study on particles suspended in an electrodynamic balance (EDB)[27] reported the transition to be in a similar temperature range. Some studies have also reported a different efflorescence crystal structure in seawater depending on the rate of decrease of RH due to different number of water molecules trapped in the dried particle.[62,63]

Here, we investigate a range of model aerosol systems in the range −20 to +25 °C that covers a significant portion of tropospheric temperature (−60 to +25 °C) for O/C ratios between 0.38 and 0.67, which are below the critical O/C < 0.92 for LLPS. We varied the organic to inorganic ratio (OIR) of the systems to estimate the effect of the organic and inorganic components on the LLPS morphology temperature-dependence. The systems studied consisted of either ammonium sulfate (AS) or sodium chloride (NaCl) as inorganics and organic acid and polyalcohol organics in an aqueous solution with OIRs ranging from 1:10 to 10:1. We also studied the binary solution of sodium chloride and water to find the effect of temperature and drying rate on the efflorescent crystal structure. This work uses a novel and low-cost, quasi-equilibrium technique to shed new light on how temperature and the OIR of these systems affect the phase separation morphology as well as the total solute concentration or conversely the SRH at which these systems undergo phase separation.

https://dx.doi.org/10.1021/acsearthspacechem.0c00114
ACS Earth Space Chem. 2020, 4, 1527−1539

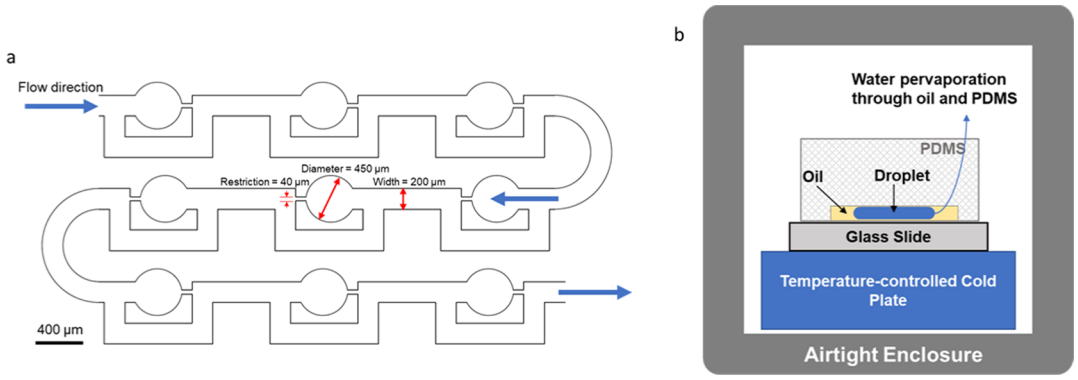

Figure 1. (a) Microfluidic static well device schematic. (b) Schematic of the microfluidic device inside the cold stage showing a pancake-shaped droplet surrounded by silicone oil in a PDMS device and the water pervaporation path through the oil and PDMS layers. For details on the microfluidic device design and fabrication, see ref 47.

MATERIALS AND METHODS

Chemicals. Solutions of AS (Fisher Scientific) and NaCl (Fisher Scientific) were prepared by dissolving crystals into high-performance liquid chromatography (HPLC)-grade water (Fisher Scientific). Organics with the O/C ratio below 0.83 were mixed with this salt solution to make experimental samples. The organics used were 3-methylglutaric acid (3-MGA, Tokyo Chemical Industry) with O/C = 0.67, poly(ethylene glycol) (PEG, molecular weight = 200 g/mol, Sigma-Aldrich) with O/C = 0.63, poly(ethylene glycol) diacrylate (PEGDia, Sigma-Aldrich) with O/C = 0.50, and poly(propylene glycol) (PPG, Sigma-Aldrich) with O/C = 0.38. The organics were mixed with the salt solution in three different ratios by mass, namely, OIR 1:10, 1:1, and 10:1.

Experiments for the ammonium sulfate and 3-MGA system were performed at four different temperatures, +25, +5, −10, and −20 °C, and three different OIRs, 1:10, 1:1, and 10:1. The same initial concentration C_0 for a given mixture system was used at all temperatures. In the AS + 3-MGA system, C_0 values were 1.42, 2.33, and 0.92 M for OIR 1:10, 1:1, and 10:1, respectively. Ammonium sulfate and other organics were studied at +25 and −20 °C at OIR 1:1. C_0 was 2.56, 0.98, and 0.67 M for AS + PEG, AS + PPG, and AS + PEGDia systems, respectively. NaCl and 3-MGA systems were studied at all three OIRs but only at +25 and −20 °C, with C_0 of 1.67, 1.15, and 0.56 M for OIR 1:10, 1:1, and 10:1, respectively.

Microfluidic Device Fabrication. The microfluidic device used for this study was adapted from ref 64 and has been used previously in refs 46 and 47 studies from our group to examine LLPS and efflorescence in different models and real systems at room temperature. Each device consists of a single inlet and outlet, along with nine microfluidic traps (Figure 1a). Each trap consists of a 200 μm wide inlet, a 450 μm diameter well, and a 40 μm wide restriction. Additionally, there is a bypass path for the carrier oil to pass through. The heights of all individual wells were measured to be between 85 and 95 μm with a KLA Tencor P16 surface profilometer.

To fabricate the device, the photomask in Figure 1a was designed in CAD software (AutoCAD, Autodesk Corp.) and printed on a vinyl transparency (CAD/Art Services Inc.). A device master on a 4 in. diameter silicon wafer was fabricated using well-established photolithography techniques[65,66] using the photomask. Subsequently, the microfluidic device was made by pouring a mix of uncured PDMS (Sylgard 184 silicone elastomer, Dow Corning Corp.) and a linking agent in a 10:1 ratio by weight into the mold. Then, the mold was degassed before baking in a 75 °C oven to cure PDMS. Next, the PDMS device was cut out from the mold, and holes were punched for the inlet and outlet. Finally, the device was sealed to a 25 × 75 × 1 mm^3 glass slide (Corning) after oxidative plasma etching of both the glass and PDMS surfaces.

Droplet Loading. The as-prepared mixed organic and inorganic aqueous sample was injected into the device to fill the microfluidic channel completely, including the wells and the bypass paths. Silicone oil (Sigma-Aldrich) was then carefully injected into the device, which scavenged all of the excess sample from the bypass channels and pushed it out through the outlet. The sample droplet already inside the well was not pushed out, since the restriction in front of the sample was small enough to prevent the droplet from squeezing through. This resulted in droplets trapped inside the wells and the rest of the channel being filled with silicone oil.

Dehydration Experiment. After droplet loading, the device was placed on the cold plate of a temperature-controlled stage (LTS 420, Linkam Scientific, U.K.) and the lid was closed. The cold stage was placed on the *XY* stage of a reflective microscope (SZX10, Olympus) and imaged using an acA1600-60gm camera (Basler) every 10 s throughout the duration of the experiment. Water from the droplets slowly diffused through the silicone oil and pervaporated through PDMS during an experiment. A schematic of the droplet trapped inside the device is shown in Figure 1b.

Trapped droplets were pancake-shaped and the volumes, V, were calculated using the method described in ref 67

$$V = \frac{\pi h^3}{6} + \frac{\pi h}{4}(D - h)\left(\frac{\pi h}{2} + D - h\right) \quad (1)$$

In eq 1, D is the diameter of the droplet and h is the channel height. The volume of the droplet is used in eq 2 to calculate the solute molarity, C (M or mol/L), of the droplet at any point during the experiment[46] by assuming that only water leaves the droplet during the experiment

$$V_0 C_0 = V_f C_f \quad (2)$$

where the subscripts 0 and f correspond to measurements taken initially and finally at the phase-transition point, respectively. The droplet solutions were always prepared with a fixed initial concentration at a given OIR and to allow for a comparison between different temperatures at the phase-transition points. The RH was not directly measured; instead,

https://dx.doi.org/10.1021/acsearthspacechem.0c00114
ACS Earth Space Chem. 2020, 4, 1527−1539

the droplet solute concentration was used to predict the RH at phase transition through a thermodynamic model that relates concentration to water activity, similar to Nandy and Dutcher[46,68] in an almost identical microfluidic setup. Using this method, the calculated efflorescence RH (ERH) of 33−35% for binary AS solution at room temperature matches closely to literature data.[69,70] We followed a similar methodology to calculate the RH of phase transitions in ternary droplets using the thermodynamic models E-AIM[71,72] (http://www.aim.env.uea.ac.uk/aim/aim.php) model II and III and AIOMFAC[73,74] (https://aiomfac.lab.mcgill.ca/model.html) between the initial droplet loading point and the point where the first phase transition (LLPS or nucleation of crystal/efflorescence) occurred. The modeling could not be extended beyond this as the droplet did not remain well-mixed and the composition of the phases was unknown after this transition point. Both models are widely used in aerosol science. E-AIM has been used previously to study mixed organic and inorganic systems in refs 75−78. AIOMFAC is also often used for studies of mixed systems,[77,79−81] with long- and medium-range interactions between organics and inorganics in aqueous solutions incorporated. For the RH calculation, 3-MGA and other organics were created as new compounds in E-AIM with activity equations defined using the group contribution method from UNIFAC. E-AIM density output was used to convert the solution molarity from eq 2 to molality and mass fraction, which was used for calculating the equilibrium RH of the droplet at the phase-transition point from both thermodynamic models. More details on the calculation methodology and results are reported in the Supporting Information.

Raman Spectroscopy (Microfluidic). For some of the samples, 2D confocal Raman spectroscopy was also performed on an AS and 3-MGA droplet trapped inside microfluidic wells at room temperature to qualitatively map the organic and salt before and after LLPS inside the droplet. The system consisted of an α 300R microscope with a UHTS300 spectrometer and a DV401 charge-coupled device detector with 600/mm grating (WITec, Germany). A 532 nm Nd:YAG laser was used for the excitation with a 100× objective (Nikon Instruments, NY). Each image had a resolution of 58 × 58 pixels with a pitch of 3 μm and an integration time of 0.1 s/pixel.

Environmental Cell Raman Microscopy. For fast drying experiments, a Raman microscope (Horiba, LabRAM HR Evolution) coupled to an environmental cell (Linkam, LTS 120) was used to collect spectra and optical images of substrate-deposited NaCl particles following deliquescence and efflorescence at both −21.0 and −25.0 ± 0.4 °C. A detailed description of the experimental setup has been described previously.[82] In this experiment, a 10% (w/w) aqueous solution of NaCl (≥99% Fischer Scientific) was passed through an atomizer (TSI Inc., model 3076) and impacted on to a hydrophobically coated (RainX) quartz substrate (Ted Pella Inc., no. 16001-1). The sample was then placed in the environmental cell and first dried under a flow of N_2 until the dew point had stabilized (measured using a hygrometer, Buck, CR-4), following which, the temperature was reduced to either −21 or −25 °C. Once equilibrium had been reached for both temperature and RH in the cell, the RH was increased to 85 ± 2% by altering the ratio of wet/dry N_2, and the particles were deliquesced. Following this, the wet N_2 line was turned off and the samples were rapidly effloresced, which took between 30 and 45 min at −21 °C and 75 and 90 min at −25 °C. Once the RH stabilized, optical images of the particle ensemble and spectra of individual particles were collected. Images were collected with an optical microscope (Olympus BX41) and a 100× super long working distance (SLWD) objective. Spectra were taken using a 532 nm Nd:YAG laser excitation source with seven exposures of 15 s each averaged to obtain individual spectra.

RESULTS

Droplets consisting of water, AS, and 3-MGA mixed with OIR 1:1 undergo LLPS while continuously dehydrating in the microfluidic trap. As shown in Figure 2a,d, following the initial

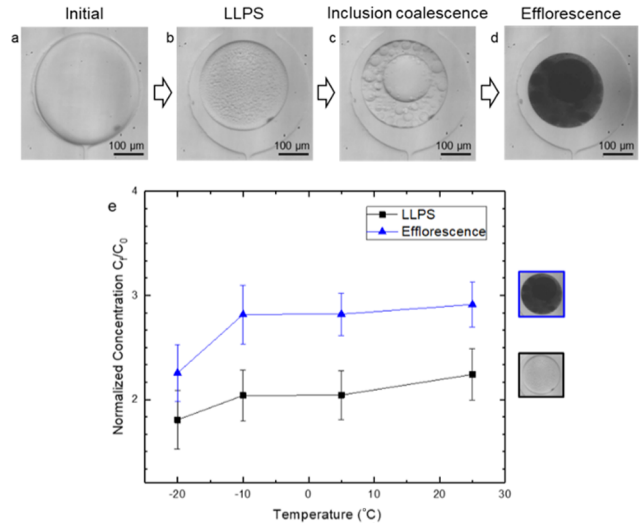

Figure 2. (a−d) Typical phase transitions in an aqueous AS and 3-MGA droplet with an organic to inorganic ratio (OIR) of 1:1 at 25 °C inside a static microfluidic trap. (e) Phase transitions reported as a function of normalized total droplet solute concentration at different temperatures. C_0 was 2.33 M for this OIR.

phase transition, the phases undergo a bulk transition into a core−shell morphology with the core comprising an inorganic-rich phase and the shell comprising an organic-rich phase. This morphology was also observed in a previous study on mixtures of AS and 3-MGA.[46] Finally, the droplets undergo efflorescence at a sufficiently low water content. Similar transitions occur at all experimental temperatures. Figure 2e shows the normalized concentration (C_f/C_0) from eq 2. Since the C_0 was constant for all droplets for a given OIR, this figure shows that droplets become comparatively more concentrated at higher temperatures before undergoing phase separation. Later in Figure 6, after application of the thermodynamic model calculator, the results are recast in terms of relative humidity. Error bars in all figures indicate the standard deviation between 3 and 9 droplets.

Figure 3a again shows a brightfield image of a trapped droplet with ammonium sulfate and 3-MGA and an OIR of 1:1 in the Raman setup. The droplet has undergone LLPS with a core−shell morphology. The contour plot in Figure 3b shows the normalized sum intensity of a 60 cm^{-1} wide band centered around the peak at 1650 cm^{-1} (for the carboxylic acid group) from 2D confocal Raman microscopy. The colors indicate that the 3-MGA is distributed mostly in the outer shell phase. The 40 cm^{-1} wide band centered around the peak at 975 cm^{-1} is indicative of the SO_4^{2-} ion, and Figure 3c shows that ammonium sulfate is present in a larger concentration in the

https://dx.doi.org/10.1021/acsearthspacechem.0c00114
ACS Earth Space Chem. 2020, 4, 1527−1539

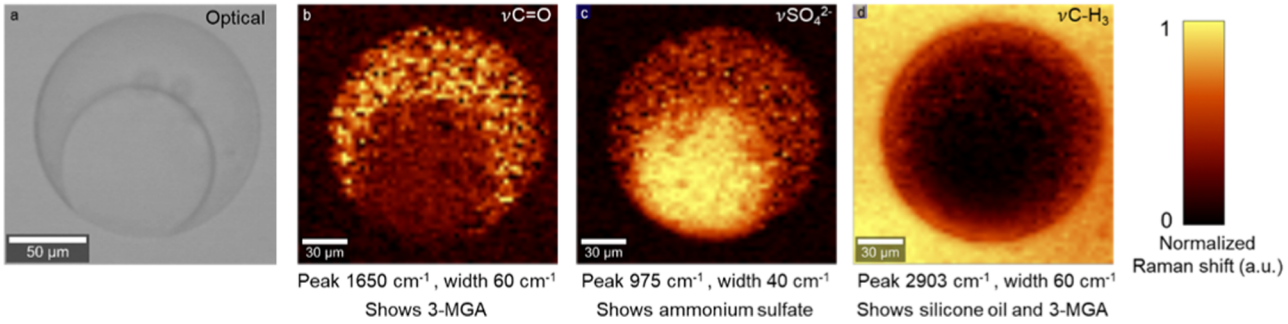

Figure 3. (a) Optical image of a phase-separated droplet of AS and 3-MGA with OIR 1:1. (b–d) Raman images for different chemical species in the sample. The spectral regions used for generating the heatmaps are indicated in the images.

core structure. Interestingly, the 60 cm^{-1} band centered around the peak at 2903 cm^{-1} indicates the presence of CH_3 groups and is present in very high concentrations around the droplet and at somewhat lower concentrations inside the outer shell structure of the droplet (Figure 3d). The outer high-concentration region is indicative of the silicone oil the droplet is immersed in, while the inner low-concentration region indicates the CH_3 groups of 3-MGA. The nonuniform halo of CH_3 encroaching inside the circular edge of the droplet in Figure 3d is an artifact of the confocal imaging system due to the pancake shape of the droplet, with a circular edge of hemispherical cross section. This causes the edge to have silicone oil at the top and bottom of the image focal plane and it shows up as nonuniformity of the signal around the edges.

Similar to OIR 1:1, droplets with AS and 3-MGA with an OIR 1:10 also undergo LLPS prior to efflorescence at all temperatures during experiments (Figure 4a–d). The

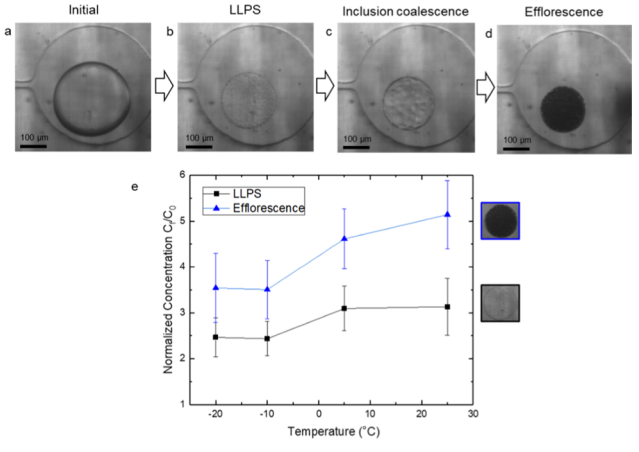

Figure 4. (a–d) Typical phase transitions in an aqueous AS and 3-MGA droplet with an organic to inorganic ratio (OIR) of 1:10 at 25 °C. The droplet undergoes LLPS but there is no subsequent core–shell formation. (e) Phase transitions reported as a function of normalized total droplet solute concentration at different temperatures. C_0 was 1.42 M for this OIR.

inorganic-rich tiny inclusions undergo some coalescence but do not form a large inner core structure. We also could not discern any differences among the inclusion coalescence behavior at different temperatures. Once again, the LLPS and efflorescence happen at lower concentrations at lower temperatures (Figure 4e).

However, in droplets of AS and 3-MGA at an OIR 10:1, no LLPS is observed (Figure 5a–d). The droplets initiate an

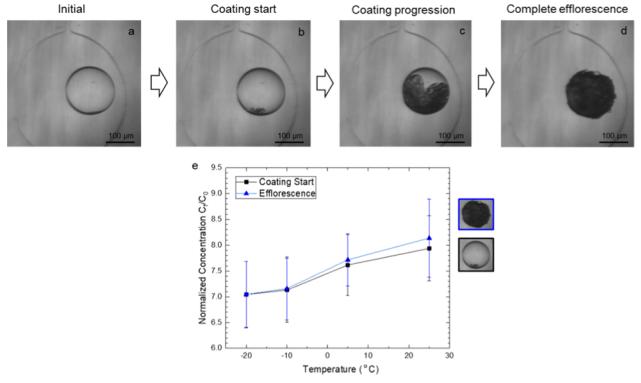

Figure 5. (a–d) Typical phase transitions in an aqueous AS and 3-MGA droplet with an organic to inorganic ratio (OIR) of 10:1 at 25 °C. The droplets do not undergo LLPS but instead a solid coating forms directly from a well-mixed state. (e) Phase transitions reported as a function of normalized total droplet solute concentration at different temperatures. C_0 was 0.92 M for this OIR.

apparent opaque coating, which progresses to efflorescence. We use the term "coating" here to indicate an event where there appears to be a progressing solid sheet growing over or through the droplet, while a portion of the droplet remains liquid. This is similar to observations in ref 46 for cases where the organic component was present in larger amounts than the salt. Even though these phase transitions are dissimilar to the other two OIRs, Figure 5e shows that there is still a temperature dependence of the RH at which the coating starts. This coating initiation event is the onset of efflorescence and called the phase-transition point in this article.

The phase-transition morphologies observed for different OIRs correspond well to a study by Song et al.[80] who studied ternary mixtures of AS as the inorganic phase and three different carboxylic acids with six carbon atoms as the organic phase. At OIR 1:1, the authors observed core–shell formation similar to our microfluidic droplet. At an OIR of 11:1, droplets effloresced with needlelike growths of ammonium sulfate being initiated from the edge of the droplet, in a similar morphology to our OIR 10:1 droplet.

The SRH values for all of these cases calculated from E-AIM are plotted as a function of temperature in Figure 6. The RH values reported here for OIR 1:1 are close to the SRH reported in similar model aerosol systems in refs 50 and 53. Additionally, these three graphs show that regardless of the OIR, the phase transitions occur at a higher RH at lower temperatures. The systems with OIR 1:1 and 1:10 have a much lower RH of phase separation than the system with OIR 10:1.

https://dx.doi.org/10.1021/acsearthspacechem.0c00114
ACS Earth Space Chem. 2020, 4, 1527–1539

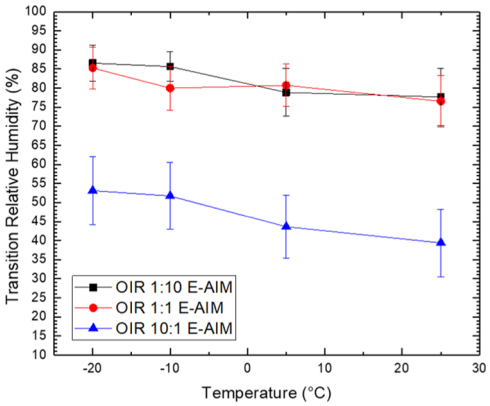

Figure 6. Relative humidities of phase transition at different organic to inorganic ratios and at different temperatures for AS + 3-MGA droplets. For the OIR 1:10 and 1:1, phase transition refers to LLPS and for OIR 10:1, phase transition refers to efflorescence by nucleation of a solid coating as there is no LLPS.

A comparison between E-AIM and AIOMFAC models for these points shows a difference of about 2−5% for the cases studied here (Figure S1 and Table ST1 in the Supporting Information). This discrepancy is well within the margin of uncertainty of our experimental methods described later on as well as the uncertainties within the models themselves related to the activity of group contribution, the temperature dependence of activity coefficients, and the temperature dependence of the density of the ternary solutions. However, we note that both methods show a comparable trend in the transition RH values as a function of temperature.

Results from experiments performed with AS as the inorganic phase and poly(ethylene glycol) with a molecular weight of 200 g/mol (PEG) as the organic phase with an OIR of 1:1 are also plotted in Figure 7a−d. The SRH of the PEG 200 system at the temperatures studied is in the range of 79−83% according to E-AIM, similar to that by You et al.[50] at room temperature for a 2:1 OIR system. The SRH is lower than that reported by Ciobanu et al.[83] in AS and PEG 400, though the differences in higher PEG molecular weight and lower O/C ratio used in their study may explain the higher tendency to phase-separate leading to larger SRH. Normalized concentrations of the LLPS transition of this system along with additional systems where the organic phase was swapped with poly(propylene glycol) (PPG) and PEG diacrylate (PEGDia) are plotted in Figure 7e. The lines in Figure 7f show that the SRH for the PPG and PEGDia systems do not increase, and perhaps even decrease with lowered temperature, but the SRH of the PEG system does rise with a reduction in temperature.

In the NaCl and 3-MGA system, there is no LLPS at any OIRs and at any temperatures studied. Instead, Figure 8a−d shows that there is crystal nucleation, which eventually leads to drying out of the complete droplet for both OIR 1:1 and 1:10. In this case, the first appearance of the crystal (i.e., the efflorescence point) was designated as the phase-transition point in our subsequent calculations. The crystal that grew at −20 °C at OIR 1:1 and 1:10 visually resembled anhydrous cubic crystals. The crystal eventually led to complete droplet efflorescence with some organic efflorescing on the crystal faces as the water evaporated. There was no LLPS in the 10:1 OIR system either, however, the crystal growth morphology was quite different with multiple crystals nucleating inside the droplet, followed by an amorphous efflorescent structure formation, as shown in Figure 8e−i. Figure 8i shows that, like the AS and 3-MGA systems, the concentration at which the initial crystal appeared is affected by the temperature of the experiment quite monotonically across all OIRs. Finally, Figure 8j shows that the RH for this phase transition also increases with lowered temperature. Unlike AS and 3-MGA, these OIR 1:1 and 1:10 systems have much lower RH of phase transition than the OIR 10:1 system. Possible reasons for this behavior are discussed later on.

A sensitivity analysis for measurement uncertainty in different parameters and their influence on the model calculated RH values were also carried out. Typical uncertainty in droplet diameter measurement was about ±5 μm due to the

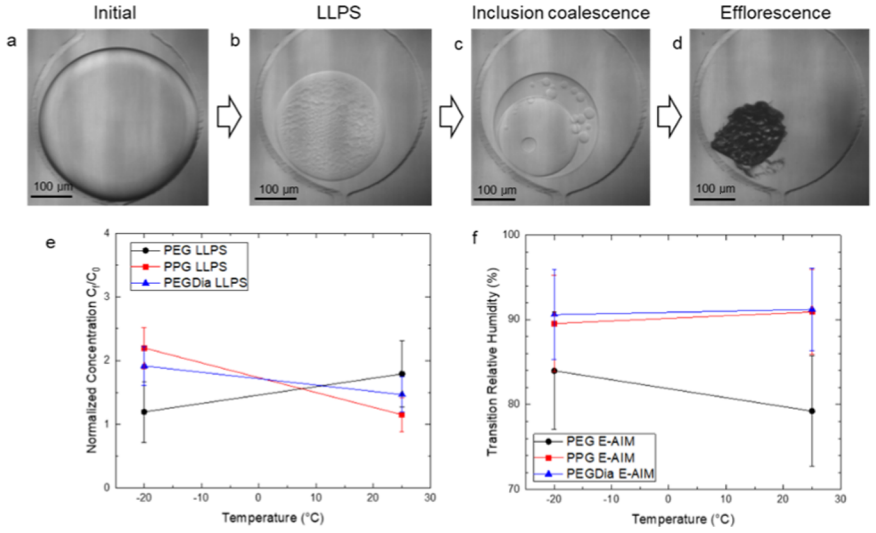

Figure 7. (a−d) Typical phase transitions in an aqueous AS and PEG droplet with an organic to inorganic ratio (OIR) of 1:1 at 25 °C. Droplets undergo LLPS followed by core−shell formation similar to the AS + 3-MGA systems. Similar behavior is observed in AS + PPG and AS + PEGDia systems as well. (e) LLPS concentrations normalized by initial concentrations for AS and PEG and PPG and PEGDia solutions as a function of temperature. C_0 was 2.56, 0.98, and 0.67 M for AS + PEG, AS + PPG, and AS + PEGDia systems, respectively. (f) Relative humidity of phase transition to an LLPS state reported for these systems at different temperatures.

https://dx.doi.org/10.1021/acsearthspacechem.0c00114
ACS Earth Space Chem. 2020, 4, 1527−1539

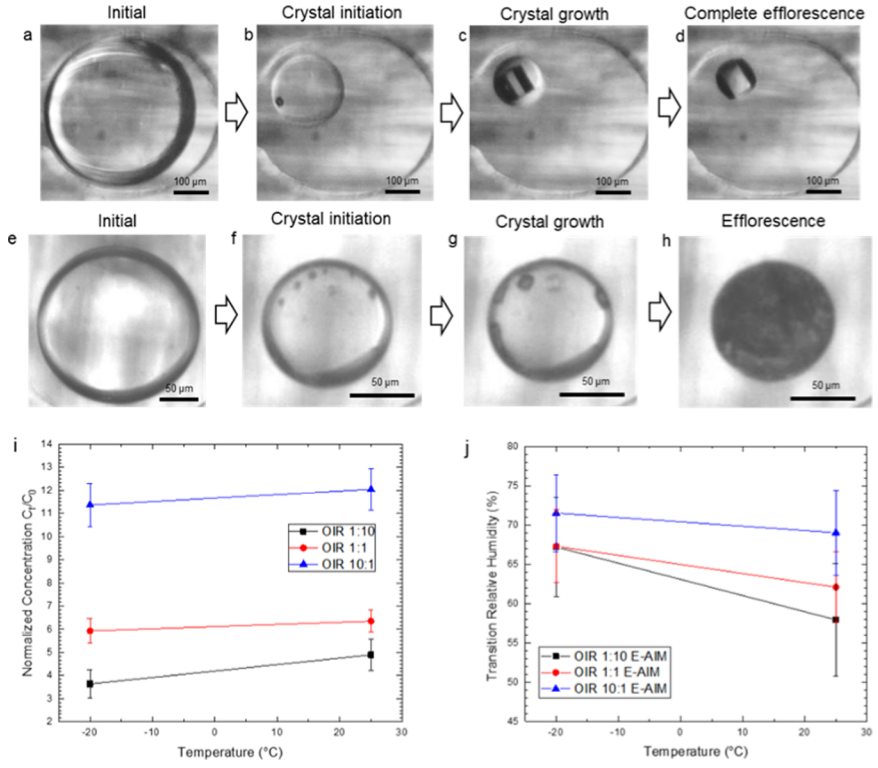

Figure 8. (a–d) Typical phase transitions in an aqueous NaCl and 3-MGA droplet with an organic to inorganic ratio (OIR) of 1:1 at 25 °C. Droplets undergo a single crystal growth at efflorescence. (e–h) Phase transitions for the same compounds at OIR 10:1 at 25 °C. Droplets undergo multiple salt crystal nucleation triggered possibly by organic efflorescence followed by complete efflorescence. (i) Normalized concentrations of NaCl and 3-MGA at initial crystal growth. C_0 was 1.67, 1.15, and 0.56 M for OIR 1:10, 1:1, and 10:1, respectively. (j) Relative humidity of initial visible crystal formation or efflorescence is reported for these systems at different temperatures.

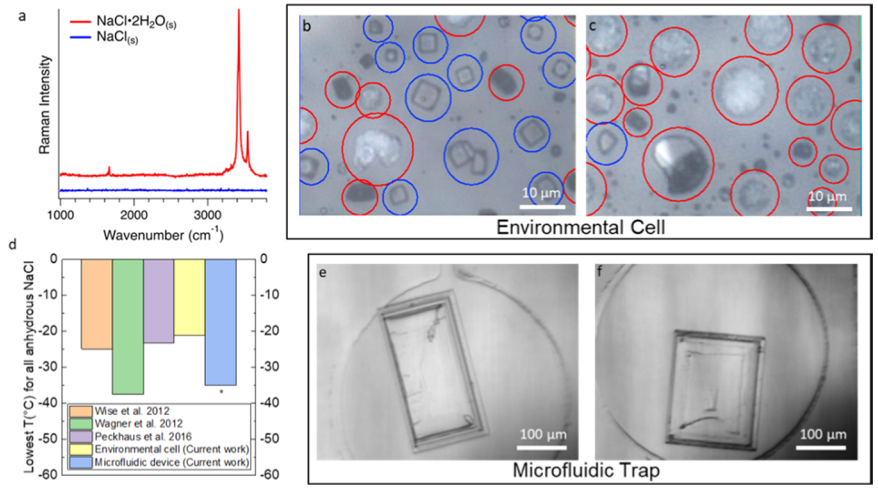

Figure 9. (a) Raman spectra of $NaCl{\cdot}2H_2O_{(s)}$ (red) and $NaCl_{(s)}$ (blue) and optical images of these particles deposited on the environmental cell substrate and fast dehydrated at (b) −21 °C and (c) −25 °C with colored circles indicating the different crystals. $NaCl_{(s)}$ efflorescence observed at (e) −25 °C and (f) −35 °C in a microfluidic well at a very slow dehydration rate. (d) Comparison of the lowest temperature at which all of the crystals were anhydrous with the literature. The asterisk over the microfluidic device column indicates the lowest-temperature experiment performed. Dihydrate crystals were not observed at this temperature. Lower temperatures may produce dihydrate crystals in this experiment but were not performed.

available camera resolution and contrast. Uncertainty was about ±1% in the initial solution concentration. Uncertainty in microfluidic channel height was about ±5 μm due to variations during fabrication between different wells in a single microfluidic device. As a result, the uncertainty in droplet final concentration was ±10.4%. This led to an average of 5.2, 4.1, and 9% uncertainties in RH prediction for AS + 3-MGA systems at OIR 1:1, 1:10, and 10:1, respectively, using the thermodynamic models. A similar analysis led to about 5.7, 4.5, and 5.2% uncertainties in RH prediction for the NaCl + 3-MGA system at OIR 1:1, 1:10, and 10:1, respectively. Another source of uncertainty in the thermodynamic models can be the density of the solutions where an error of about 0.01 g/cm^3 leads to an error in concentration prediction of 6% on average

https://dx.doi.org/10.1021/acsearthspacechem.0c00114
ACS Earth Space Chem. 2020, 4, 1527–1539

and final RH prediction error of about 3, 2.5, and 5.2% for the AS + 3-MGA systems at OIR 1:1, 1:10, and 10:1, respectively.

Experiments were also performed to investigate the effect of temperature and dehydration rate on the efflorescence of binary sodium chloride water solution. Faster dehydration rate experiments (∼2.5% RH/min at −21 °C and ∼1% RH/min at −25 °C) were performed on the environmental cell. Figure 9b,c shows that at −21 °C, 15.3 ± 0.1% of the droplets formed $NaCl{\cdot}2H_2O_{(s)}$, which went up to 98.5 ± 0.6% at −25 °C. Raman spectra (Figure 9a) were used to confirm the hydration state of the particles. Slow dehydration rate experiments were performed over a period of about 5−6 days in the microfluidic trap, and Figure 9e,f shows that at both −25 and −35 °C, the efflorescent form was $NaCl_{(s)}$.

DISCUSSION

Previous studies on model aerosols have shown that the SRH is affected only weakly by temperature and molecular weight of the organic compound[53] and instead dominated by the O/C ratio of the organic compound. While no direct comparisons are possible between the studies due to the vastly different molar ratios of solutes and dehydration rates as well as specific temperatures studied, the trend in the results can be commented upon. For example, efflorescence RH of AS with different organics shows a slightly increasing or constant trend at lower temperatures.[84,85] Similarly, the deliquescence RH of mixed organic and AS systems show an increasing trend with reduced temperatures.[86] Here, in a similar fashion, we see a clear trend toward higher SRH at lower temperatures for the AS + 3-MGA systems studied. This could be explained by reduced solubility of pure organics as well as salts at lower temperatures.[87] However, this trend is not always present across all systems studied and it cannot be positively asserted that reducing the temperature of LLPS would lead to a higher SRH across the board, which is in agreement with ref 53. More likely, the type of organic including the functional group (alcohol, carboxylic acid, etc.), molecular weight, as well as the solubility of the organic in the salty droplet leads to a nuanced behavior with no generalizable trend in terms of temperature dependence.

While we did not see any dependence of the actual series of morphological phase transitions on temperature, we did see different morphologies depending on the droplet OIR. Droplets with more salt than organic resulted in small inclusions containing the salt-rich phase formed inside the droplet, which did not fully separate from the outer organic phase. We noticed this same trend where metastable inclusions in the OIR 1:10 droplets formed after LLPS, which coalesced to form larger inclusions but not a central core before efflorescence. Fard et al.[88] previously observed temperature- and drying rate-dependent inorganic ion diffusivity and organic inclusion coalescence in mixed AS and carminic acid droplets at OIR 1:3 after LLPS. We could not discern any temperature dependence of the inclusion coalescence in our drops. This could be due to several reasons. The fastest rate of dehydration in our experiments was an order of magnitude slower than the slowest rate reported by Fard et al. Also, the OIR and the organic acid itself are very different, which perhaps suggests that a coalescence temperature dependence is possible at a different temperature rate and OIR in our system. We also cannot rule out the possibility that we missed out on small variations in coalescence behavior due to limited resolution and contrast in the droplets. In systems with comparable amounts of salt and acid, fully separated core−shell formation is observed. For droplets that contained significantly larger amounts of acid than salt, it was observed previously[46,80] that the droplet did not spontaneously change phase all at once, but rather a progressive solidification or coating formed through crystallization from a given point on the droplet surface. Similar behavior was also observed here for OIR 10:1, where the crystallization started from a given point on the droplet and no LLPS was observed. Finally, in addition to the phase-transition events, a noticeable difference in the critical value of the SRH was observed here for systems with different OIRs. In AS + 3-MGA systems containing more organic than salt, specifically for OIR 10:1, the ERH was much lower than the SRH reported for the systems with OIR 1:1 and 1:10. This is probably caused by the efflorescence of the AS phase as has been previously suggested by Song et al.[80] After the initiation of the coating at a low RH, the whole droplet effloresces quickly, which we believe is the organic crystallizing heterogeneously on the already effloresced AS since the amount of organic is 10 times larger in the droplet than the salt.

Experiments performed on the NaCl and 3-MGA systems showed a completely different phase-transition morphology in contrast with AS, as expected. For the systems studied here, the NaCl droplets did not undergo any LLPS but started an anhydrous crystal growth before efflorescence, resulting in an organic coating on and around the salt crystal. It has been shown previously[89] that AS has a larger SRH than NaCl in a large study of mixed salt and organic droplets. This indicates that AS has a larger tendency of salting out the organics from the droplet than NaCl, thus favoring LLPS over crystallization, potentially explained by the Hofmeister series[90] where the abilities of ions to salt out proteins are classified in a linear order. Since there was no LLPS in our study, we were able to report the concentration and RH at which the NaCl crystal first appeared or the start of efflorescence as a function of temperature. At OIR 10:1, multiple NaCl crystals started efflorescing at a larger RH close to the DRH of pure NaCl (∼75%) than the other OIRs, indicating possible heterogeneous nucleation of NaCl due to formation of a few organic crystals. Studies have shown that the presence of a nucleating surface is able to crystallize inorganic salts close to their DRH.[91,92] Following this, droplets rapidly formed an opaque amorphous coating without significant crystal growth or droplet dehydration, indicating an organic coating due to the comparatively large amount of organic in the droplet. This contrasts with the RH of the crystallization for the AS system where the droplets crystallized closer to the ERH of pure AS, indicating that the AS crystallized first. More work is needed to understand this differing behavior between the two systems. At all OIRs, the appearance of the crystal was at a lower concentration (and higher RH) at lower temperatures, indicating again perhaps the reduced solubility of the components as the temperature reduced. It is interesting to note that we observed the anhydrous form of the NaCl crystal during the experiment rather than the thermodynamically stable dihydrous form, which resembles a circular shape with irregularities.[27]

We noticed a similar behavior in binary NaCl water systems. In this case, NaCl droplets without a ternary organic phase and dehydrated at two very different rates showed a dependence of the rate of change of RH as well as the droplet surroundings on the crystal structure formed. The slower dehydrating micro-

https://dx.doi.org/10.1021/acsearthspacechem.0c00114
ACS Earth Space Chem. 2020, 4, 1527−1539

fluidic droplets formed cubic $NaCl_{(s)}$ crystals down to −35 °C, whereas the faster dehydrating environmental cell droplets formed irregular $NaCl{\cdot}2H_2O_{(s)}$ crystals even at −25 °C. This is perhaps a combined effect of the vastly different dehydration rates as well as the droplet surroundings in the two setups. It has been reported previously[93] that at higher rates of dehydration, NaCl droplets form a dendritic and irregular crystal structure upon nucleation, whereas slower dehydration leads to the single cubic crystal structure. The authors postulated that slower dehydration leads to related slower homogenous nucleation and growth, which favors the singular anhydrous crystal rather than rapid crystal growth, inducing trapped water molecules and a random structure. It has also been theorized previously that the presence of heterogeneous nucleation sites on a solid−droplet interface and higher dehydration rates are capable of inducing the transition to $NaCl{\cdot}2H_2O_{(s)}$ at higher temperatures by reducing the energy barrier for the transition to this state.[27,94] No consensus exists in the literature about the temperature range of this transition in droplets with the range being dependent on size, dehydration rate, and overall method; for example, in the study by Wagner et al.,[94] the highest temperature for the transition was about −37.45 °C, whereas Peckhaus et al.[27] and Wise et al. reported −23 and −21 °C, respectively, for the same transition. This highlights the fact that while speculative, differences in droplet size, shape, substrates, as well as the other factors discussed above could all potentially be contributing factors while comparing the transition temperatures between the methods presented here. The rate of dehydration has also been shown to be a major factor affecting the morphology of efflorescing particles in previous studies on seawater[62,63] as well as studies on pharmaceutical compounds[95,96] and could be the biggest cause of the different crystal structures at the same temperature seen here and needs to be investigated further.

CONCLUSIONS

We used a PDMS-based microfluidic device to trap aqueous chemical systems relevant to atmospheric aerosol droplets. The device was placed inside a hermetically sealed temperature-controlled cell, and the temperature of the cell was held fixed throughout the experiment. The droplets dehydrated as water pervaporated through the PDMS and left the microfluidic device in a quasi-static manner. Droplet solute concentrations were calculated based on optical microscopy data and the concentration was used with the E-AIM model to calculate relative humidities at the first phase transition. Concentrations and relative humidities of phase changes of the droplet were reported as a function of temperatures ranging from +25 to −20 °C. Additionally, a study on the effect of dehydration rates on efflorescent crystal structure was performed on binary sodium chloride and water systems with two vastly different dehydration rates.

It was observed that the changes in phase occurred at a lower total solute concentration at lower temperatures in most droplets. The relative humidity of the first phase transition in all systems was calculated using the E-AIM model, showing that the SRH increased as the phase-transition temperature was lowered. The SRH results are somewhat contradictory to previous studies with similar systems, which show weak or no appreciable trend in SRH at lower temperatures. While the SRH for supermicron droplets does not depend on their size, slow time scales for water transport may play a role in phase transitions in a microfluidic well when compared to other methods. However, the trend of lower total solute concentration and higher RH at phase separation with lowered temperature is clearly visible in the AS and 3-MGA system. The effect of the organic to inorganic ratio on SRH was also shown to be temperature-dependent. Rate of dehydration and the droplet surroundings also had an impact on the phase transition with NaCl crystals formed at slower dehydration rates in our microfluidic device favoring the metastable anhydrous form than the dihydrous form which was predominant at faster dehydration rates at the same temperature on a cold plate device.

A shortcoming in the methodology includes the need to use a thermodynamic model to calculate the equilibrium RH of the droplets instead of directly measuring it. This adds to the experimental uncertainties (droplet concentration, volume, and density) by introducing modeling related uncertainties for activities of the mixed organic and inorganic systems at low temperatures. Future device designs with either a controlled RH environment surrounding the PDMS device or flow channels that allow for droplet rehydration to identify deliquescence behavior for further benchmarking to known transitions would be helpful to overcome this shortcoming.

This study provides a novel look at the temperature, OIR, and dehydration rate dependence of phase changes in atmospheric aerosol relevant chemical systems using a low-cost microfluidic apparatus. Ultimately, the temperature- and RH-dependent phase of aerosol droplets influences various cloud and atmospheric processes, such as gas-particle partitioning of certain compounds, cloud condensation nuclei activation, optical properties, and heterogeneous chemistry. Future work with environmental samples would involve studying environmental samples of sea surface microlayer, seawater, and sea spray aerosol samples in our microfluidic setup to observe their phase-transition temperature dependence.

ASSOCIATED CONTENT

Supporting Information

The Supporting Information is available free of charge at https://pubs.acs.org/doi/10.1021/acsearthspacechem.0c00114.

Modeling details for E-AIM and AIOMFAC; results from both model calculations; statistics from the dihydrous/anhydrous NaCl efflorescence experiment at high dehydration rate and temporal droplet volume curves in microfluidic wells for ternary systems (PDF)

Time-lapse video of a ternary aqueous droplet with ammonium sulfate and 3-methylglutaric acid with an organic to inorganic ratio by mass of 10:1 at a temperature of 25 °C (MP4)

Time-lapse video of a ternary aqueous droplet with ammonium sulfate and 3-methylglutaric acid with an organic to inorganic ratio by mass of 1:1 at a temperature of 25 °C (MP4)

Time-lapse video of a ternary aqueous droplet with ammonium sulfate and 3-methylglutaric acid with an organic to inorganic ratio by mass of 1:1 at a temperature of 25 °C (MP4)

https://dx.doi.org/10.1021/acsearthspacechem.0c00114
ACS Earth Space Chem. 2020, 4, 1527−1539

AUTHOR INFORMATION

Corresponding Author

Cari S. Dutcher − *Department of Mechanical Engineering and Department of Chemical Engineering & Materials Science, University of Minnesota, Twin Cities, Minneapolis, Minnesota 55455, United States;* orcid.org/0000-0003-4325-9197; Email: cdutcher@umn.edu

Authors

Priyatanu Roy − *Department of Mechanical Engineering, University of Minnesota, Twin Cities, Minneapolis, Minnesota 55455, United States*

Liora E. Mael − *Department of Chemistry, University of California, San Diego, La Jolla, California 92037, United States*

Iaroslav Makhnenko − *Department of Mechanical Engineering, University of Minnesota, Twin Cities, Minneapolis, Minnesota 55455, United States*

Robert Martz − *Department of Mechanical Engineering, University of Minnesota, Twin Cities, Minneapolis, Minnesota 55455, United States*

Vicki H. Grassian − *Department of Chemistry, University of California, San Diego, La Jolla, California 92037, United States;* orcid.org/0000-0001-5052-0045

Complete contact information is available at: https://pubs.acs.org/10.1021/acsearthspacechem.0c00114

Author Contributions

The manuscript was written through the contributions of all authors. All authors have given approval to the final version of the manuscript.

Notes

The authors declare no competing financial interest.

ACKNOWLEDGMENTS

This work was supported by NSF through the NSF Center for Aerosol Impacts on Chemistry of the Environment (CAICE), an NSF Funded Center for Chemical Innovation (CHE-1801971), including support for P.R., NSF Graduate Research Fellowship Program (DGE-1650112) for support of L.M., and the NSF CAREER (AGS-1554936), including support of I.M. Portions of this work were conducted in the Minnesota Nano Center, which is supported by the National Science Foundation through the National Nano Coordinated Infrastructure Network (NNCI) under Award Number ECCS-2025124. Any opinions, findings, and conclusions or recommendations expressed in this material are those of the authors and do not necessarily reflect the views of the National Science Foundation. Finally, the authors would like to thank Shweta Narayan and Shihao Liu for their advice on microfluidic fabrication and experimental methods.

ABBREVIATIONS

AS, ammonium sulfate; LLPS, liquid−liquid phase separation; NaCl, sodium chloride; OIR, organic to inorganic ratio; RH, relative humidity; SRH, separation relative humidity; 3-MGA, 3-methylglutaric acid; PEG, poly(ethylene glycol); PPG, poly(propylene glycol); PEGDia, poly(ethylene glycol) diacrylate

REFERENCES

(1) Pandis, S. N.; Wexler, A. S.; Seinfeld, J. H. Dynamics of Tropospheric Aerosols. *J. Phys. Chem. A.* **1995**, *99*, 9646−9659.

(2) Seinfeld, J. H.; Pandis, S. N.; Noone, K. Atmospheric Chemistry and Physics: From Air Pollution to Climate Change. *Phys. Today* **2006**, DOI: 10.1063/1.882420.

(3) Heintzenberg, J. Fine Particles in the Global Troposphere A Review. *Tellus B* **1989**, *2*, 149−160.

(4) Yu, H.; Kaufman, Y. J.; Chin, M.; Feingold, G.; Remer, L. A.; Anderson, T. L.; Balkanski, Y.; Bellouin, N.; Boucher, O.; Christopher, S.; DeCola, P.; Kahn, R.; Koch, D.; Loeb, N.; Reddy, M. S.; Schulz, M.; Takemura, T.; Zhou, M. A Review of Measurement-Based Assessments of the Aerosol Direct Radiative Effect and Forcing. *Atmos. Chem. Phys.* **2006**, *6*, 613−666.

(5) Haywood, J.; Boucher, O. Estimates of the Direct and Indirect Radiative Forcing Due to Tropospheric Aerosols: A Review. *Rev. Geophys.* **2000**, *38*, 513−543.

(6) Lohmann, U.; Feichter, J. Global Indirect Aerosol Effects: A Review. *Atmos. Chem. Phys.* **2005**, *5*, 715−737.

(7) Stocker, T. F.; Qin, D.; Plattner, G. K.; Tignor, M.; Allen, S. K.; Boschung, J.; Nauels, A.; Xia, Y.; Bex, V.; Midgley, P. M. *IPCC, 2013: Climate Change 2013: The Physical Science Basis. Contribution of Working Group I to the Fifth Assessment Report of the Intergovernmental Panel on Climate Change*; Cambridge University Press: U.K., 2013.

(8) Fitzgerald, J. W. Marine Aerosols: A Review. *Atmos. Environ., Part A* **1991**, 533−545.

(9) Shepherd, J. M. A Review of Current Investigations of Urban-Induced Rainfall and Recommendations for the Future. *Earth Interact.* **2005**, *9*, 1−27.

(10) Kulmala, M.; Vehkamäki, H.; Petäjä, T.; Dal Maso, M.; Lauri, A.; Kerminen, V. M.; Birmili, W.; McMurry, P. H. Formation and Growth Rates of Ultrafine Atmospheric Particles: A Review of Observations. *J. Aerosol Sci.* **2004**, *35*, 143−176.

(11) Després, V.; Huffman, J. A.; Burrows, S. M.; Hoose, C.; Safatov, A.; Buryak, G.; Fröhlich-Nowoisky, J.; Elbert, W.; Andreae, M.; Pöschl, U.; Jaenicke, R. Primary Biological Aerosol Particles in the Atmosphere: A Review. *Tellus B* **2012**, *64*, No. 15598.

(12) O'Dowd, C. D.; Smith, M. H.; Consterdine, I. E.; Lowe, J. A. Marine Aerosol, Sea-Salt, and the Marine Sulphur Cycle: A Short Review. *Atmos. Environ.* **1997**, *31*, 73−80.

(13) O'Dowd, C. D.; Facchini, M. C.; Cavalli, F.; Ceburnis, D.; Mircea, M.; Decesari, S.; Fuzzi, S.; Yoon, Y. J.; Putaud, J.-P. Biogenically Driven Organic Contribution to Marine Aerosol. *Nature* **2004**, *431*, 676−680.

(14) Cochran, R. E.; Ryder, O. S.; Grassian, V. H.; Prather, K. A. Sea Spray Aerosol: The Chemical Link between the Oceans, Atmosphere, and Climate. *Acc. Chem. Res.* **2017**, 599−604.

(15) DeMott, P. J.; Hill, T. C. J.; McCluskey, C. S.; Prather, K. A.; Collins, D. B.; Sullivan, R. C.; Ruppel, M. J.; Mason, R. H.; Irish, V. E.; Lee, T.; Hwang, C. Y.; Rhee, T. S.; Snider, J. R.; McMeeking, G. R.; Dhaniyala, S.; Lewis, E. R.; Wentzell, J. J. B.; Abbatt, J.; Lee, C.; Sultana, C. M.; Ault, A. P.; Axson, J. L.; Diaz Martinez, M.; Venero, I.; Santos-Figueroa, G.; Stokes, M. D.; Deane, G. B.; Mayol-Bracero, O. L.; Grassian, V. H.; Bertram, T. H.; Bertram, A. K.; Moffett, B. F.; Franc, G. D. Sea Spray Aerosol as a Unique Source of Ice Nucleating Particles. *Proc. Natl. Acad. Sci. U.S.A* **2016**, *113*, 5797−5803.

(16) Marcolli, C.; Krieger, U. K. Phase Changes during Hygroscopic Cycles of Mixed Organic/Inorganic Model Systems of Tropospheric Aerosols. *J. Phys. Chem. A* **2006**, *110*, 1881−1893.

(17) Freedman, M. A. Phase Separation in Organic Aerosol. *Chem. Soc. Rev.* **2017**, *46*, 7694−7705.

(18) Martin, S. T. Phase Transitions of Aqueous Atmospheric Particles. *Chem. Rev.* **2000**, *100*, 3403−3453.

(19) Lesins, G.; Chylek, P.; Lohmann, U. A Study of Internal and External Mixing Scenarios and Its Effect on Aerosol Optical Properties and Direct Radiative Forcing. *J. Geophys. Res.: Atmos.* **2002**, *107*, No. 4094.

(20) Fard, M. M.; Krieger, U. K.; Peter, T. Shortwave Radiative Impact of Liquid-Liquid Phase Separation in Brown Carbon Aerosols. *Atmos. Chem. Phys.* **2018**, *18*, 13511−13530.

(21) Hodas, N.; Zuend, A.; Mui, W.; Flagan, R. C.; Seinfeld, J. H. Influence of Particle-Phase State on the Hygroscopic Behavior of

Mixed Organic-Inorganic Aerosols. *Atmos. Chem. Phys.* **2015**, *15*, 5027−5045.
(22) Cosman, L. M.; Bertram, A. K. Reactive Uptake of N2O5 on Aqueous H 2so4 Solutions Coated with 1-Component and 2-Component Monolayers. *J. Phys. Chem. A* **2008**, *112*, 4625−4635.
(23) Cosman, L. M.; Knopf, D. A.; Bertram, A. K. N2O5 Reactive Uptake on Aqueous Sulfuric Acid Solutions Coated with Branched and Straight-Chain Insoluble Organic Surfactants. *J. Phys. Chem. A* **2008**, *112*, 2386−2396.
(24) Altaf, M. B.; Dutcher, D. D.; Raymond, T. M.; Freedman, M. A. Effect of Particle Morphology on Cloud Condensation Nuclei Activity. *ACS Earth Space Chem.* **2018**, *2*, 634−639.
(25) Wise, M. E.; Baustian, K. J.; Koop, T.; Freedman, M. A.; Jensen, E. J.; Tolbert, M. A. Depositional Ice Nucleation onto Crystalline Hydrated NaCl Particles: A New Mechanism for Ice Formation in the Troposphere. *Atmos. Chem. Phys.* **2012**, *12*, 1121−1134.
(26) Wagner, R.; Möhler, O. Heterogeneous Ice Nucleation Ability of Crystalline Sodium Chloride Dihydrate Particles. *J. Geophys. Res.: Atmos.* **2013**, *118*, 4610−4622.
(27) Peckhaus, A.; Kiselev, A.; Wagner, R.; Duft, D.; Leisner, T. Temperature-Dependent Formation of NaCl Dihydrate in Levitated NaCl and Sea Salt Aerosol Particles. *J. Chem. Phys.* **2016**, *145*, No. 244503.
(28) You, Y.; Renbaum-Wolff, L.; Carreras-Sospedra, M.; Hanna, S. J.; Hiranuma, N.; Kamal, S.; Smith, M. L.; Zhang, X.; Weber, R. J.; Shilling, J. E.; Dabdub, D.; Martin, S. T.; Bertram, A. K. Images Reveal That Atmospheric Particles Can Undergo Liquid-Liquid Phase Separations. *Proc. Natl. Acad. Sci. U.S.A.* **2012**, *109*, 13188−13193.
(29) Tang, I. N.; Munkelwitz, H. R. Composition and Temperature Dependence of the Deliquescence Properties of Hygroscopic Aerosols. *Atmos. Environ., Part A* **1993**, *27*, 467−473.
(30) Gorkowski, K.; Beydoun, H.; Aboff, M.; Walker, J. S.; Reid, J. P.; Sullivan, R. C. Advanced Aerosol Optical Tweezers Chamber Design to Facilitate Phase-Separation and Equilibration Timescale Experiments on Complex Droplets. *Aerosol Sci. Technol.* **2016**, *50*, 1327−1341.
(31) Sobanska, S.; Coeur, C.; Maenhaut, W.; Adams, F. SEM-EDX Characterisation of Tropospheric Aerosols in the Negev Desert (Israel). *J. Atmos. Chem.* **2003**, *44*, 299−322.
(32) Veghte, D. P.; Bittner, D. R.; Freedman, M. A. Cryo-Transmission Electron Microscopy Imaging of the Morphology of Submicrometer Aerosol Containing Organic Acids and Ammonium Sulfate. *Anal. Chem.* **2014**, *86*, 2436−2442.
(33) Takahama, S.; Gilardoni, S.; Russell, L. M. Single-Particle Oxidation State and Morphology of Atmospheric Iron Aerosols. *J. Geophys. Res.* **2008**, *113*, No. D22202.
(34) McMurry, P. H.; Litchy, M.; Huang, P. F.; Cai, X.; Turpin, B. J.; Dick, W. D.; Hanson, A. Elemental Composition and Morphology of Individual Particles Separated by Size and Hygroscopicity with the TDMA. *Atmos. Environ.* **1996**, *30*, 101−108.
(35) Zardini, A. A.; Sjogren, S.; Marcolli, C.; Krieger, U. K.; Gysel, M.; Weingartner, E.; Baltensperger, U.; Peter, T. A Combined Particle Trap/HTDMA Hygroscopicity Study of Mixed Inorganic/Organic Aerosol Particles. *Atmos. Chem. Phys.* **2008**, *8*, 5589−5601.
(36) Cheng, Y.; Su, H.; Koop, T.; Mikhailov, E.; Pöschl, U. Size Dependence of Phase Transitions in Aerosol Nanoparticles. *Nat. Commun.* **2015**, *6*, No. 5923.
(37) Zielinski, A. T.; Gallimore, P. J.; Griffiths, P. T.; Jones, R. L.; Seshia, A. A.; Kalberer, M. Measuring Aerosol Phase Changes and Hygroscopicity with a Microresonator Mass Sensor. *Anal. Chem.* **2018**, *90*, 9716−9724.
(38) Schindelholz, E.; Tsui, L. K.; Kelly, R. G. Hygroscopic Particle Behavior Studied by Interdigitated Array Microelectrode Impedance Sensors. *J. Phys. Chem. A* **2014**, *118*, 167−177.
(39) Arenas, K. J. L.; Schill, S. R.; Malla, A.; Hudson, P. K. Deliquescence Phase Transition Measurements by Quartz Crystal Microbalance Frequency Shifts. *J. Phys. Chem. A* **2012**, *116*, 7658−7667.
(40) Bateman, A. P.; Belassein, H.; Martin, S. T. Impactor Apparatus for the Study of Particle Rebound: Relative Humidity and Capillary Forces. *Aerosol Sci. Technol.* **2014**, *48*, 42−52.
(41) Bateman, A. P.; Gong, Z.; Liu, P.; Sato, B.; Cirino, G.; Zhang, Y.; Artaxo, P.; Bertram, A. K.; Manzi, A. O.; Rizzo, L. V.; Souza, R. A. F.; Zaveri, R. A.; Martin, S. T. Sub-Micrometre Particulate Matter Is Primarily in Liquid Form over Amazon Rainforest. *Nat. Geosci.* **2016**, *9*, 34−37.
(42) Bateman, A. P.; Gong, Z.; Harder, T. H.; De Sá, S. S.; Wang, B.; Castillo, P.; China, S.; Liu, Y.; O'Brien, R. E.; Palm, B. B.; Shiu, H. W.; Cirino, G. G.; Thalman, R.; Adachi, K.; Lizabeth Alexander, M.; Artaxo, P.; Bertram, A. K.; Buseck, P. R.; Gilles, M. K.; Jimenez, J. L.; Laskin, A.; Manzi, A. O.; Sedlacek, A.; Souza, R. A. F.; Wang, J.; Zaveri, R.; Martin, S. T. Anthropogenic Influences on the Physical State of Submicron Particulate Matter over a Tropical Forest. *Atmos. Chem. Phys.* **2017**, *17*, 1759−1773.
(43) Jain, S.; Petrucci, G. A. A New Method to Measure Aerosol Particle Bounce Using a Cascade Electrical Low Pressure Impactor. *Aerosol Sci. Technol.* **2015**, *49*, 390−399.
(44) McMurry, P. H. Chapter 17 A Review of Atmospheric Aerosol Measurements. *Dev. Environ. Sci.* **2002**, *1*, 443−517.
(45) Bleier, B. J.; Anna, S. L.; Walker, L. M. Microfluidic Droplet-Based Tool to Determine Phase Behavior of a Fluid System with High Composition Resolution. *J. Phys. Chem. B* **2018**, *122*, 4067−4076.
(46) Nandy, L.; Dutcher, C. S. Phase Behavior of Ammonium Sulfate with Organic Acid Solutions in Aqueous Aerosol Mimics Using Microfluidic Traps. *J. Phys. Chem. B* **2018**, *122*, 3480−3490.
(47) Nandy, L.; Liu, S.; Gunsbury, C.; Wang, X.; Pendergraft, M. A.; Prather, K. A.; Dutcher, C. S. Multistep Phase Transitions in Sea Surface Microlayer Droplets and Aerosol Mimics Using Microfluidic Wells. *ACS Earth Space Chem.* **2019**, *3*, 1260−1267.
(48) Brubaker, T.; Polen, M.; Cheng, P.; Ekambaram, V.; Somers, J.; Anna, S. L.; Sullivan, R. C. Development and Characterization of a "Store and Create" Microfluidic Device to Determine the Heterogeneous Freezing Properties of Ice Nucleating Particles. *Aerosol Sci. Technol.* **2020**, *54*, 79−93.
(49) Shim, J. U.; Cristobal, G.; Link, D. R.; Thorsen, T.; Jia, Y.; Piattelli, K.; Fraden, S. Control and Measurement of the Phase Behavior of Aqueous Solutions Using Microfluidics. *J. Am. Chem. Soc.* **2007**, *129*, 8825−8835.
(50) You, Y.; Renbaum-Wolff, L.; Bertram, A. K. Liquid−Liquid Phase Separation in Particles Containing Organics Mixed with Ammonium Sulfate, Ammonium Bisulfate, Ammonium Nitrate or Sodium Chloride. *Atmos. Chem. Phys.* **2013**, *13*, 11723−11734.
(51) Song, M.; Marcolli, C.; Krieger, U. K.; Zuend, A.; Peter, T. Liquid-Liquid Phase Separation in Aerosol Particles: Dependence on O:C, Organic Functionalities, and Compositional Complexity. *Geophys. Res. Lett.* **2012**, *39*, No. L19801.
(52) Song, M.; Maclean, A. M.; Huang, Y.; Smith, N. R.; Blair, S. L.; Laskin, J.; Laskin, A.; DeRieux, W.-S. W.; Li, Y.; Shiraiwa, M.; Nizkorodov, S. A.; Bertram, A. K. Liquid−Liquid Phase Separation and Viscosity within Secondary Organic Aerosol Generated from Diesel Fuel Vapors. *Atmos. Chem. Phys.* **2019**, *19*, 12515−12529.
(53) You, Y.; Bertram, A. K. Effects of Molecular Weight and Temperature on Liquid−Liquid Phase Separation in Particles Containing Organic Species and Inorganic Salts. *Atmos. Chem. Phys.* **2015**, *15*, 1351−1365.
(54) Song, M.; Ham, S.; Andrews, R. J.; You, Y.; Bertram, A. K. Liquid-Liquid Phase Separation in Organic Particles Containing One and Two Organic Species: Importance of the Average O:C. *Atmos. Chem. Phys.* **2018**, *18*, 12075−12084.
(55) Ham, S.; Bin Babar, Z.; Bong Lee, J.; Lim, H. J.; Song, M. Liquid-Liquid Phase Separation in Secondary Organic Aerosol Particles Produced from α-Pinene Ozonolysis and α-Pinene Photo-oxidation with/without Ammonia. *Atmos. Chem. Phys.* **2019**, *19*, 9321−9331.
(56) Ott, E.-J. E.; Tackman, E. C.; Freedman, M. A. Effects of Sucrose on Phase Transitions of Organic/Inorganic Aerosols. *ACS Earth Space Chem.* **2020**, *4*, 591−601.

https://dx.doi.org/10.1021/acsearthspacechem.0c00114
ACS Earth Space Chem. 2020, 4, 1527−1539

(57) Zobrist, B.; Marcolli, C.; Pedernera, D. A.; Koop, T. Do Atmospheric Aerosols Form Glasses? *Atmos. Chem. Phys.* **2008**, *8*, 5221−5244.
(58) Chen, Q.; Farmer, D. K.; Schneider, J.; Zorn, S. R.; Heald, C. L.; Karl, T. G.; Guenther, A.; Allan, J. D.; Robinson, N.; Coe, H.; Kimmel, J. R.; Pauliquevis, T.; Borrmann, S.; Pöschl, U.; Andreae, M. O.; Artaxo, P.; Jimenez, J. L.; Martin, S. T. Mass Spectral Characterization of Submicron Biogenic Organic Particles in the Amazon Basin. *Geophys. Res. Lett.* **2009**, *36*, No. L20806.
(59) Sun, Y.; Wang, Z.; Dong, H.; Yang, T.; Li, J.; Pan, X.; Chen, P.; Jayne, J. T. Characterization of Summer Organic and Inorganic Aerosols in Beijing, China with an Aerosol Chemical Speciation Monitor. *Atmos. Environ.* **2012**, *51*, 250−259.
(60) Jimenez, J. L.; Canagaratna, M. R.; Donahue, N. M.; Prevot, A. S. H.; Zhang, Q.; Kroll, J. H.; DeCarlo, P. F.; Allan, J. D.; Coe, H.; Ng, N. L.; Aiken, A. C.; Docherty, K. S.; Ulbrich, I. M.; Grieshop, A. P.; Robinson, A. L.; Duplissy, J.; Smith, J. D.; Wilson, K. R.; Lanz, V. A.; Hueglin, C.; Sun, Y. L.; Tian, J.; Laaksonen, A.; Raatikainen, T.; Rautiainen, J.; Vaattovaara, P.; Ehn, M.; Kulmala, M.; Tomlinson, J. M.; Collins, D. R.; Cubison, M. J.; Dunlea, E. J.; Huffman, J. A.; Onasch, T. B.; Alfarra, M. R.; Williams, P. I.; Bower, K.; Kondo, Y.; Schneider, J.; Drewnick, F.; Borrmann, S.; Weimer, S.; Demerjian, K.; Salcedo, D.; Cottrell, L.; Griffin, R.; Takami, A.; Miyoshi, T.; Hatakeyama, S.; Shimono, A.; Sun, J. Y.; Zhang, Y. M.; Dzepina, K.; Kimmel, J. R.; Sueper, D.; Jayne, J. T.; Herndon, S. C.; Trimborn, A. M.; Williams, L. R.; Wood, E. C.; Middlebrook, A. M.; Kolb, C. E.; Baltensperger, U.; Worsnop, D. R. Evolution of Organic Aerosols in the Atmosphere. *Science* **2009**, *326*, 1525−1529.
(61) Cziczo, D. J.; Abbatt, J. P. D. Infrared Observations of the Response of NaCl, MgCl2, NH4HSO4, and NH4NO3 Aerosols to Changes in Relative Humidity from 298 to 238 K. *J. Phys. Chem. A* **2000**, *104*, 2038−2047.
(62) Tong, H. J.; Qian, Z. G.; Reid Jonathan, P.; Zhang, Y. H. High Temporal and Spatial Resolution Measurements of the Rapid Efflorescence of Sea Salt Droplets. *Acta Phys.-Chim. Sin.* **2011**, *27*, 2521−2527.
(63) Qian, Z. G.; Wang, F.; Zheng, Y. X.; Yu, J. Y.; Zhang, Y. H. Crystallization Kinetics of Sea-Salt Aerosols Studied by High-Speed Photography. *Chin. Sci. Bull.* **2012**, *57*, 591−594.
(64) Sun, M.; Bithi, S. S.; Vanapalli, S. A. Microfluidic Static Droplet Arrays with Tuneable Gradients in Material Composition. *Lab Chip* **2011**, *11*, 3949−3952.
(65) Vuong, S. M. *A Microfluidic Platform for the Control and Analysis of Phase Transitions in Concentrating Droplets*; Carnegie Mellon University, 2014.
(66) McDonald, J. C.; Duffy, D. C.; Anderson, J. R.; Chiu, D. T.; Wu, H.; Schueller, O. J. A.; Whitesides, G. M. Fabrication of Microfluidic Systems in Poly(Dimethylsiloxane). *Electrophoresis* **2000**, *21*, 27−40.
(67) Vuong, S. M.; Anna, S. L. Tuning Bubbly Structures in Microchannels. *Biomicrofluidics* **2012**, *6*, No. 022004.
(68) Nandy, L.; Dutcher, C. S. Isotherm-Based Thermodynamic Model for Solute Activities of Asymmetric Electrolyte Aqueous Solutions. *J. Phys. Chem. A* **2017**, *121*, 6957−6965.
(69) Cziczo, D. J.; Nowak, J. B.; Hu, J. H.; Abbatt, J. P. D. Infrared Spectroscopy of Model Tropospheric Aerosols as a Function of Relative Humidity: Observation of Deliquescence and Crystallization. *J. Geophys. Res.: Atmos.* **1997**, *102*, 18843−18850.
(70) Schlenker, J. C.; Malinowski, A.; Martin, S. T.; Hung, H. M.; Rudich, Y. Crystals Formed at 293 K by Aqueous Sulfate-Nitrate-Ammonium-Proton Aerosol Particles. *J. Phys. Chem. A* **2004**, *108*, 9375−9383.
(71) Clegg, S. L.; Ho, S. S.; Chan, C. K.; Brimblecombe, P. Thermodynamic Properties of Aqueous (NH4)2SO4 to High Supersaturation as a Function of Temperature. *J. Chem. Eng. Data* **1995**, *40*, 1079−1090.
(72) Friese, E.; Ebel, A. Temperature Dependent Thermodynamic Model of the System H +-NH4+-Na+-SO42-NO3-Cl−H2O. *J. Phys. Chem. A* **2010**, *114*, 11595−11631.
(73) Zuend, A.; Marcolli, C.; Luo, B. P.; Peter, T. A Thermodynamic Model of Mixed Organic-Inorganic Aerosols to Predict Activity Coefficients. *Atmos. Chem. Phys.* **2008**, *8*, 4559−4593.
(74) Ganbavale, G.; Zuend, A.; Marcolli, C.; Peter, T. Improved AIOMFAC Model Parameterisation of the Temperature Dependence of Activity Coefficients for Aqueous Organic Mixtures. *Atmos. Chem. Phys.* **2015**, *15*, 447−493.
(75) Hanford, K. L.; Mitchem, L.; Reid, J. P.; Clegg, S. L.; Topping, D. O.; McFiggans, G. B. Comparative Thermodynamic Studies of Aqueous Glutaric Acid, Ammonium Sulfate and Sodium Chloride Aerosol at High Humidity. *J. Phys. Chem. A* **2008**, *112*, 9413−9422.
(76) Pope, F. D.; Dennis-Smither, B. J.; Griffiths, P. T.; Clegg, S. L.; Cox, R. A. Studies of Single Aerosol Particles Containing Malonic Acid, Glutaric Acid, and Their Mixtures with Sodium Chloride. I. Hygroscopic Growth. *J. Phys. Chem. A* **2010**, *114*, 5335−5341.
(77) Lei, T.; Zuend, A.; Wang, W. G.; Zhang, Y. H.; Ge, M. F. Hygroscopicity of Organic Compounds from Biomass Burning and Their Influence on the Water Uptake of Mixed Organic Ammonium Sulfate Aerosols. *Atmos. Chem. Phys.* **2014**, *14*, 11165−11183.
(78) Estillore, A. D.; Morris, H. S.; Or, V. W.; Lee, H. D.; Alves, M. R.; Marciano, M. A.; Laskina, O.; Qin, Z.; Tivanski, A. V.; Grassian, V. H. Linking Hygroscopicity and the Surface Microstructure of Model Inorganic Salts, Simple and Complex Carbohydrates, and Authentic Sea Spray Aerosol Particles. *Phys. Chem. Chem. Phys.* **2017**, *19*, 21101−21111.
(79) Zuend, A.; Marcolli, C.; Peter, T.; Seinfeld, J. H. Computation of Liquid-Liquid Equilibria and Phase Stabilities: Implications for RH-Dependent Gas/Particle Partitioning of Organic-Inorganic Aerosols. *Atmos. Chem. Phys.* **2010**, *10*, 7795−7820.
(80) Song, M.; Marcolli, C.; Krieger, U. K.; Zuend, A.; Peter, T. Liquid-Liquid Phase Separation and Morphology of Internally Mixed Dicarboxylic Acids/Ammonium Sulfate/Water Particles. *Atmos. Chem. Phys.* **2012**, *12*, 2691−2712.
(81) Zuend, A.; Seinfeld, J. H. Modeling the Gas-Particle Partitioning of Secondary Organic Aerosol: The Importance of Liquid-Liquid Phase Separation. *Atmos. Chem. Phys.* **2012**, *12*, 3857−3882.
(82) Mael, L. E.; Busse, H.; Grassian, V. H. Measurements of Immersion Freezing and Heterogeneous Chemistry of Atmospherically Relevant Single Particles with Micro-Raman Spectroscopy. *Anal. Chem.* **2019**, *91*, 11138−11145.
(83) Ciobanu, V. G.; Marcolli, C.; Krieger, U. K.; Weers, U.; Peter, T. Liquid-Liquid Phase Separation in Mixed Organic/Inorganic Aerosol Particles. *J. Phys. Chem. A* **2009**, *113*, 10966−10978.
(84) Onasch, T. B.; McGraw, R.; Imre, D. Temperature-Dependent Heterogeneous Efflorescence of Mixed Ammonium Sulfate/Calcium Carbonate Particles. *J. Phys. Chem. A* **2000**, *104*, 10797−10806.
(85) Wise, M. E.; Baustian, K. J.; Tolbert, M. A. Internally Mixed Sulfate and Organic Particles as Potential Ice Nuclei in the Tropical Tropopause Region. *Proc. Natl. Acad. Sci. U.S.A.* **2010**, *107*, 6693−6698.
(86) Brooks, S. D.; Wise, M. E.; Cushing, M.; Tolbert, M. A. Deliquescence Behavior of Organic/Ammonium Sulfate Aerosol. *Geophys. Res. Lett.* **2002**, *29*, 23-1−24-1.
(87) Perry, R. H.; Green, D. W., Eds. *Perry's Chemical Engineers' Handbook*, 8th ed.; McGraw-Hill, 2007.
(88) Fard, M. M.; Krieger, U. K.; Peter, T. Kinetic Limitation to Inorganic Ion Diffusivity and to Coalescence of Inorganic Inclusions in Viscous Liquid−Liquid Phase-Separated Particles. *J. Phys. Chem. A* **2017**, *121*, 9284−9296.
(89) You, Y.; Smith, M. L.; Song, M.; Martin, S. T.; Bertram, A. K. Liquid-Liquid Phase Separation in Atmospherically Relevant Particles Consisting of Organic Species and Inorganic Salts. *Int. Rev. Phys. Chem.* **2014**, *33*, 43−77.
(90) Hofmeister, F. Zur Lehre von Der Wirkung Der Salze - Zweite Mittheilung. *Arch. Exp. Pathol. Pharmakol.* **1888**, *24*, 247−260.
(91) Davis, R. D.; Lance, S.; Gordon, J. A.; Ushijima, S. B.; Tolbert, M. A. Contact Efflorescence as a Pathway for Crystallization of

Atmospherically Relevant Particles. *Proc. Natl. Acad. Sci. U.S.A.* **2015**, *112*, 15815−15820.
(92) Davis, R. D.; Tolbert, M. A. Crystal Nucleation Initiated by Transient Ion-Surface Interactions at Aerosol Interfaces. *Sci. Adv.* **2017**, *3*, No. e1700425.
(93) Utoft, A.; Kinoshita, K.; Bitterfield, D. L.; Needham, D. Manipulating Single Microdroplets of NaCl Solutions: Solvent Dissolution, Microcrystallization, and Crystal Morphology. *Langmuir* **2018**, *34*, 3626−3641.
(94) Wagner, R.; Möhler, O.; Schnaiter, M. Infrared Optical Constants of Crystalline Sodium Chloride Dihydrate: Application to Study the Crystallization of Aqueous Sodium Chloride Solution Droplets at Low Temperatures. *J. Phys. Chem. A* **2012**, *116*, 8557−8571.
(95) Ono, M.; Tozuka, Y.; Oguchi, T.; Yamamura, S.; Yamamoto, K. Effects of Dehydration Temperature on Water Vapor Adsorption and Dissolution Behavior of Carbamazepine. *Int. J. Pharm.* **2002**, *239*, 1−12.
(96) Kachrimanis, K.; Griesser, U. J. Dehydration Kinetics and Crystal Water Dynamics of Carbamazepine Dihydrate. *Pharm. Res.* **2012**, *29*, 1143−1157.

https://dx.doi.org/10.1021/acsearthspacechem.0c00114
ACS Earth Space Chem. 2020, 4, 1527−1539